Inducing Charge Separation in Solid-State Two-Dimensional Hybrid Perovskites through the Incorporation of Organic Charge-Transfer Complexes

Gélvez-Rueda, María C.; Van Gompel, Wouter T.M.; Herckens, Roald; Lutsen, Laurence; Vanderzande, Dirk; Grozema, Ferdinand C.

DOI
10.1021/acs.jpclett.9b03746

Publication date
2020

Document Version
Final published version

Published in
The Journal of Physical Chemistry Letters

THE JOURNAL OF PHYSICAL CHEMISTRY Letters

pubs.acs.org/JPCL

Letter

Inducing Charge Separation in Solid-State Two-Dimensional Hybrid Perovskites through the Incorporation of Organic Charge-Transfer Complexes

María C. Gélvez-Rueda, Wouter T. M. Van Gompel, Roald Herckens, Laurence Lutsen, Dirk Vanderzande, and Ferdinand C. Grozema*

Cite This: J. Phys. Chem. Lett. 2020, 11, 824−830

Read Online

ACCESS | Metrics & More | Article Recommendations | Supporting Information

ABSTRACT: Two-dimensional (2D) hybrid perovskites make up an emerging class of materials for optoelectronic applications in which inorganic octahedral layers are separated by nonconductive large organic cations. This leads to a high-dimensional and dielectric confinement and hence a high exciton binding energy, which severely limits their application in devices in which charge carrier separation is required. In this work, we achieve improved charge separation by replacing nonconductive organic cations with organic charge-transfer complexes consisting of a pyrene donor and a tetracyanoquinodimethane acceptor. Steady-state absorption measurements show that these materials exhibit optical features that match with the absorption of the organic charge-transfer complexes. Using microwave conductivity and femtosecond transient absorption, we show that photoexcitation of these charge-transfer states leads to long-lived mobile charges in the inorganic layers. While the efficiency of charge separation is relatively low, these experiments demonstrate that it is possible to induce charge separation in solid-state 2D perovskites by engineering the organic layer.

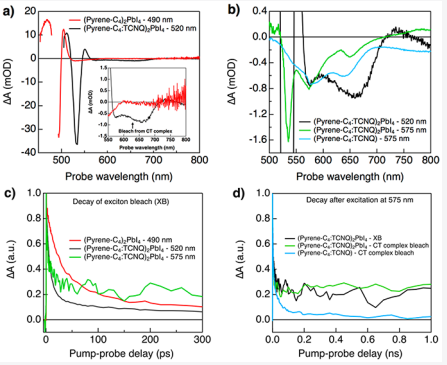

Two-dimensional (2D) hybrid organic−inorganic perovskites are tunable semiconductor materials formed by layers of inorganic metal halide octahedral $[MX_6]^{2-}$ separated by large organic cations $[A]^+$.[1,2] So far, the role of the organic cation in these materials has been mostly defined by the use of nonfunctional organic molecules such as *n*-alkylammonium, phenylethylammonium, benzylammonium, and guanidinium.[2] As a result, the organic cations act as a nonconductive barrier while the charge carrier transport occurs exclusively in the inorganic octahedral layers.[3−5] In these layers, the charge carriers experience a strong dimensional and dielectric confinement (exciton binding energies of ∼200−400 meV) that results in formation of stable excitons at room temperature.[4,6,7] This is desirable for light-emitting diodes (LEDs) and nanolasers but limits the application of 2D hybrid perovskites in optoelectronic devices in which charge separation is required, for instance, solar cells, photodetectors, and photocatalysts. It has been shown that the high exciton binding energy that charge carriers experience in the inorganic layers can be decreased by introducing organic cations with high polarizability that influence the dielectric environment in the 2D perovskite.[8,9] On the contrary, an interesting alternative to generate free charge carriers is to introduce functional organic compounds that can either accept or donate electrons to dissociate the excitons.[10] It has been shown theoretically that introducing strong functional organic molecules into 2D hybrid perovskites results in localized electronic orbitals/bands in both the inorganic octahedral layer and the organic molecules. In principle, this could result in charge separation and subsequent transport of free charge carriers.[10] Experimentally, few 2D hybrid perovskites have been synthesized using functional organic cations such as conjugated organic molecules, chromophores, and molecular complexes.[11−18] However, in none of these previous studies were the charge- or energy-transfer characteristics in these materials considered. Only in some recent studies was an indication of access to triplet states in the organic molecules reported.[13,19−21]

In a previous work, we reported the formation of 2D perovskite thin films in which electron-donating moieties pyrene-alkylammonium (pyrene-C_n) and the full charge-transfer (CT) complex of this donor molecule combined with the strong electron acceptor tetracyanoquinodimethane (TCNQ) were introduced between the inorganic octahedral layers.[22,23] We reported steady-state optical absorption measurements in which the donor-only compound, (Pyrene-C_4)$_2$PbI$_4$, exhibits a spectrum similar to that of 2D materials with nonfunctionalized organic cations.[24−26] In contrast, (pyrene-C_4:TCNQ)$_2$PbI$_4$ exhibits absorption features from

Received: December 17, 2019
Accepted: January 16, 2020
Published: January 16, 2020

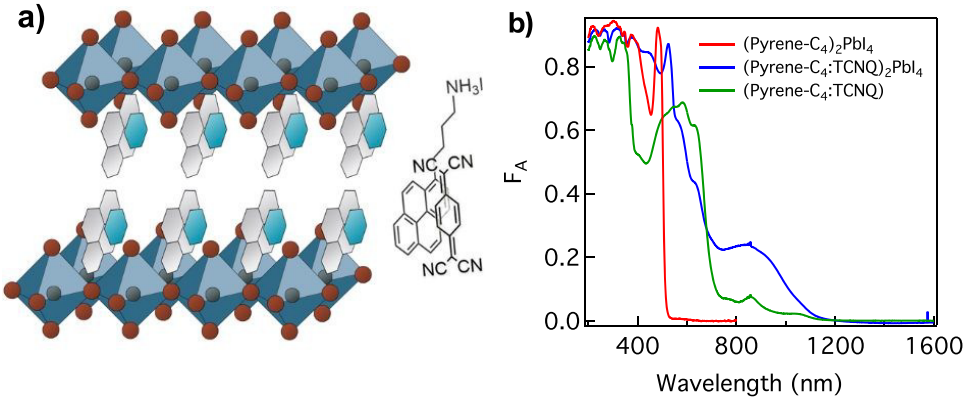

Figure 1. Schematic representation/illustration of the structure and steady-state absorption. (a) Schematic representation/illustration of the structure of the charge-transfer complex (pyrene-C_4:TCNQ) between the inorganic octahedral layers in (pyrene-C_4:TCNQ)$_2PbI_4$. Reproduced with permission from ref 22. Copyright 2019 Royal Society of Chemistry. (b) Steady-state absorption of (pyrene-C_4)$_2PbI_4$, (TCNQ:pyrene-C_4)$_2PbI_4$, and (TCNQ:pyrene-C_4) CT organic salt.

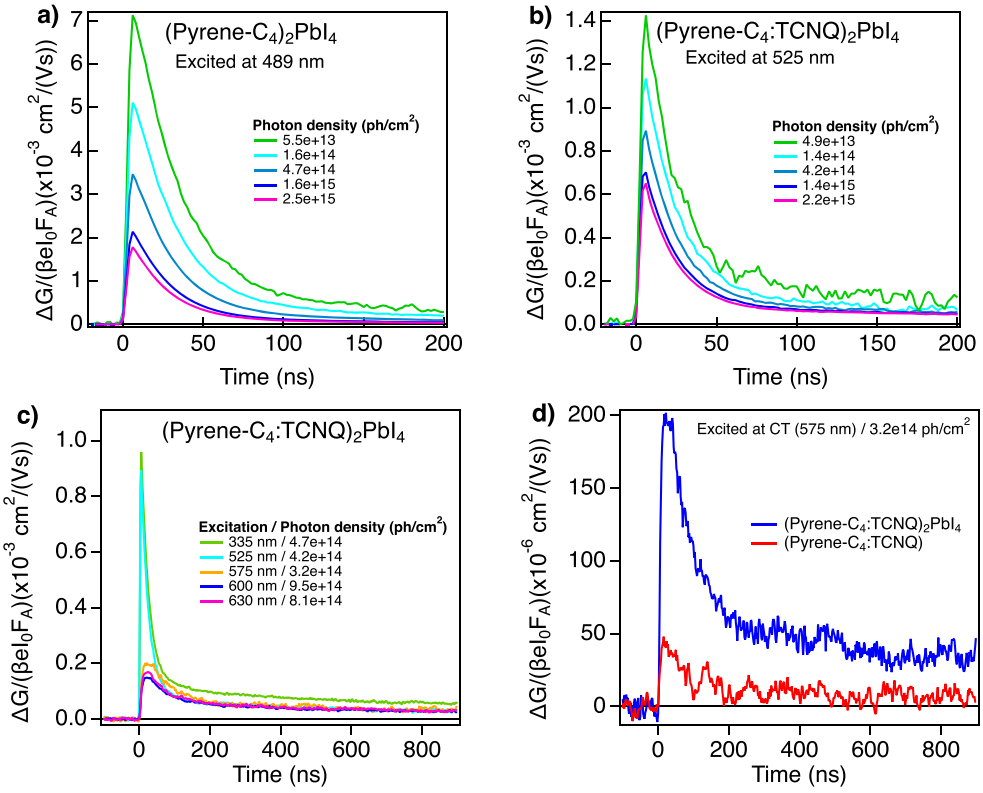

Figure 2. Photoconductivity TRMC experiments. (a and b) Photoconductivity as a function of the photon intensity for (pyrene-C_4)$_2PbI_4$ and (TCNQ:pyrene-C_4)$_2PbI_4$, respectively. (c) Photoconductivity of (TCNQ:pyrene-C_4)$_2PbI_4$ at different excitation wavelengths, with a photon intensity of ~4 × 10^{14} photons/cm^2. (d) Comparison of the photoconductivity of (TCNQ:pyrene-C_4)$_2PbI_4$ and (TCNQ:pyrene-C_4) CT organic salt by exciting the CT state at 575 nm, with a photon intensity ~4 × 10^{14} photons/cm^2.

the organic charge-transfer (CT) complex: two broad charge-transfer bands, one between 550 and 750 nm and another one at ~800 nm.[27] These additional absorption features indicate processes that are different from those in nonfunctionalized 2D perovskites. In this work, we have studied the photophysical properties of these compounds using laser-induced time-resolved microwave conductivity (TRMC) and femtosecond transient absorption (fs-TA) measurements. By microwave conductivity, we show that the charge carriers in (pyrene-C_4)$_2PbI_4$ are still confined to the inorganic layers (weak photoconductivity signal and fast decay kinetics).[6] In contrast, the photoconductivity of (pyrene-C_4:TCNQ)$_2PbI_4$ exhibits a long-lived signal (~1−4 μs) attributed to charge-separated holes transferred from the (pyrene-C_4:TCNQ) CT complex into the inorganic octahedral layers, while the electrons stay localized in the TCNQ molecules. This was confirmed by the transient absorption (TA) measurements by direct photo-excitation of the high-energy CT state at 575 nm. While the efficiency of charge separation is relatively low, this shows for the first time that inclusion of charge-transfer complexes

https://dx.doi.org/10.1021/acs.jpclett.9b03746
J. Phys. Chem. Lett. 2020, 11, 824−830

between the inorganic layers in 2D perovskites can result in charge transfer and long-lived free carrier conduction in solid-state 2D hybrid perovskites. The time scale of free charge carrier conduction (1−4 μs) is in the relevant range for application in optoelectronic devices.

We have previously reported the synthesis and characterization of the 2D hybrid perovskite thin films with the donor-only pyrene modified with an alkyl chain, (pyrene-C_4)$_2$$PbI_4$, and the CT complex formed with strong electron acceptor tetracyanoquinodimethane (TCNQ), (pyrene-C_4:TCNQ)$_2$$PbI_4$.[22] The formation of 2D perovskite structures was confirmed by X-ray diffraction by identifying the (0 0 l) reflections characteristic of preferential growth along the (1 1 0) direction parallel to the substrate (Figure S1).[22,28] In addition, Figure S1 shows that the 2D (pyrene-C_4:TCNQ)$_2$$PbI_4$ perovskite does not exhibit reflections that match with the XRD pattern of the CT (pyrene:TCNQ) organic complex. This confirms that there is no detectable presence of segregated CT complex that is not part of the layered structure. However, the full structure has not been resolved as 2D single crystals have not been synthesized. In fact, upon the introduction of TCNQ, we have been able to synthesize only one-dimensional (pyrene-C_4)PbI_3*(TCNQ) single crystals as shown previously.[29] Efforts are ongoing to determine the full 2D structure. A schematic representation/illustration of the structure of 2D (pyrene-C_4:TCNQ)$_2$$PbI_4$ is shown in Figure 1a.

In addition, we have shown that the steady-state absorption of (pyrene-C_4)$_2$$PbI_4$ exhibits the typical absorption features of 2D perovskites: an excitonic transition at ∼490−520 nm and a continuous band absorption at higher energies (see Figure 1b).[24−26] Interestingly, apart from the excitonic features typical of 2D perovskites, the compound (pyrene-C_4:TCNQ)$_2$$PbI_4$ exhibits absorption features derived from the (pyrene-C_4:TCNQ) CT complex: two broad charge-transfer bands, one between ∼550 and 700 nm and another at ∼850 nm (see Figure 1b).[27] These additional features are clearly seen in Figure 1b where the steady-state absorption of the control compounds (pyrene-C_4)$_2$$PbI_4$ and the nonperovskite (pyrene-C_4:TCNQ) CT complex is also plotted for comparison. Apart from the additional absorption features, the main excitonic transition in (pyrene-C_4:TCNQ)$_2$$PbI_4$ (∼530 nm) is red-shifted compared to that of (pyrene-C_4)$_2$$PbI_4$ (490 nm). This shift is attributed to structural rearrangements in the inorganic octahedral layers to accommodate the bulky TCNQ molecules.[29] Red-shifts in 2D perovskites have been previously associated with a decrease in the geometric distortion of the inorganic $[PbI_4]^{2-}$ octahedra.[25] With regard to the photoluminescence emission, we have previously shown that from (pyrene-C_4:TCNQ)$_2$$PbI_4$ it is only observed emission from the excitonic transition at ∼530 nm and no emission from the CT state is observed (see Figure S2).[22]

The photoinduced conductivity obtained from microwave (TRMC) measurements upon excitation at the maximum of the excitonic transition (∼490−530 nm) is shown in panels a and b of Figure 2 for (pyrene-C_4)$_2$$PbI_4$ and (pyrene-C_4:TCNQ)$_2$$PbI_4$, respectively. For (pyrene-C_4)$_2$$PbI_4$, the photoinduced conductivity shown in Figure 2a exhibits the typical features observed for 2D perovskites with nonfunctional organic cations: a photoinduced conductivity maximum, in terms of the product of mobility and yield of dissociation ($\mu\varphi = \Delta G/\beta e I_0 F_A$), on the order of 0.01 $cm^2\ V^{-1}\ s^{-1}$, where the dissociation yield is generally very small for such 2D perovskites. The conductivity signal is due to the small fraction of free charges and is characterized by a fast recombination decay (lifetime of <50 ns) due to the large dimensional and dielectrical confinement.[6] In contrast, the photoconductivity of (pyrene-C_4:TCNQ)$_2$$PbI_4$ shown in Figure 2b is slightly lower directly after the excitation pulse and exhibits two distinct decay times. The magnitude of the photoconductivity is most likely affected by the introduction of TCNQ on the inorganic layers (seen in the absorption spectra), which ultimately also affects the intrinsic charge mobility and photoconductivity signal. With regard to the two distinct decay times, first, a fast initial decay is seen that matches with the decay of electron−hole pairs in the inorganic octahedral layers similar to the decay in 2D perovskites with nonfunctional chromophores. Second, this decay is followed by a long-lived tail from ∼1 to 4 μs (see Figure S3) that is still present at high photon intensities, indicating that it is not significantly reduced by second-order recombination effects as observed for (pyrene-C_4)$_2$$PbI_4$ in Figure 2a.

To clarify the origin of the long-lived signal, we performed additional experiments by photoexciting (pyrene-C_4:TCNQ)$_2$$PbI_4$ at a series of wavelengths: 335 nm to excite the pyrene molecules, 525 nm to excite the excitonic peak, and 575, 600, and 630 nm to directly excite the CT states in the organic CT complex. Figure 2c shows that excitation at energies above the CT state (335 and 525 nm) results in a combination of two very different decay times as described above. In contrast, direct excitation of the CT state (575, 600, and 630 nm) leads to a photoconductivity signal that is an order of magnitude smaller but with only a slow decay that matches the slow decay component observed after excitation at higher energies (335 and 525 nm). As a control measurement, the photoinduced conductivity of the (pyrene-C_4:TCNQ) CT complex (without the perovskite component) is shown in Figure 2d. As one can see, both the maximum photoconductivity and the carrier lifetime are much smaller than in (pyrene-C_4:TCNQ)$_2$$PbI_4$. This is in agreement with typical photoconductivity measurements on organic materials where low short-lived transients are common.[30] From these measurements, we conclude that the long-lived photoconductivity component in (pyrene-C_4:TCNQ)$_2$$PbI_4$ is not from transport in the organic charge-transfer complex but due to enhanced charge separation leading to long-lived positive charges in the inorganic $[PbI_6]^-$ octahedral layers. This suggests that by excitation of the (pyrene-C_4:TCNQ) CT complex, it is possible to transfer holes to the inorganic octahedral layer while the electrons stay localized in the TCNQ molecules. It should be noted that the overall yield of these charge pairs separated across the built-in organic−inorganic interface is rather low and can be observed only because of the high sensitivity of the microwave technique.

The photoconductivity of (pyrene-C_4:TCNQ)$_2$$PbI_4$ is shown as a function of temperature in Figure S4. If free charge carriers were generated efficiently by charge separation, the photoconductivity would increase at low temperatured. This is a result of a higher charge mobility due to reduced lattice scattering.[6] However, this is not the case for (pyrene-C_4:TCNQ)$_2$$PbI_4$ where the photoconductivity increases at higher temperatures. We attribute this to more efficient dissociation of charges by charge transfer from the (pyrene-C_4:TCNQ) CT complex. As the charge-transfer process in (pyrene-C_4:TCNQ) is known to be extremely fast, we

https://dx.doi.org/10.1021/acs.jpclett.9b03746
J. Phys. Chem. Lett. 2020, 11, 824−830

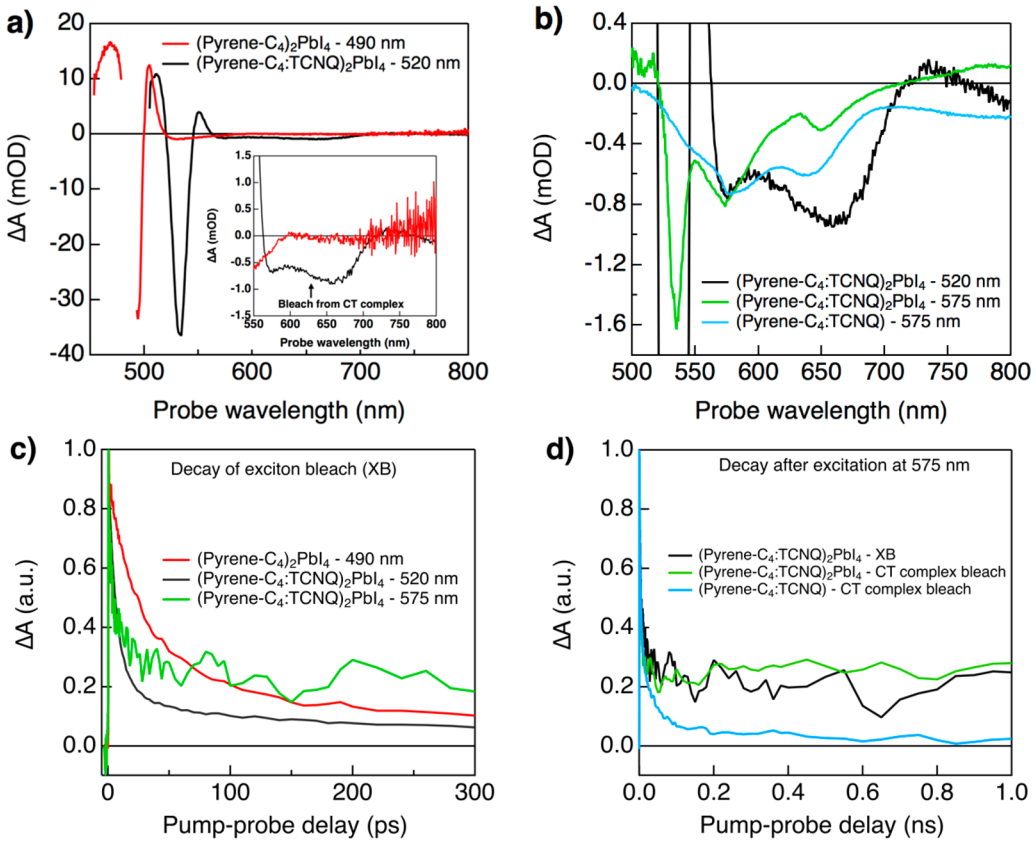

Figure 3. Femtosecond transient absorption experiments. (a) TA spectra of $(pyrene\text{-}C_4)_2PbI_4$ and $(pyrene\text{-}C_4{:}TCNQ)_2PbI_4$ excited at the excitonic peak (490 and 520 nm, respectively). (b) TA spectra of $(pyrene\text{-}C_4{:}TCNQ)_2PbI_4$ and (pyrene-C_4:TCNQ) CT salt excited at the CT state (575 nm). (c) Temporal decay kinetics of the exciton bleach (XB) of $(pyrene\text{-}C_4)_2PbI_4$ (~500 nm) and $(pyrene\text{-}C_4{:}TCNQ)_2PbI_4$ (~530 nm) upon excitation at the excitonic peak (490 and 520 nm, respectively) and the CT state (575 nm). Photon fluence of $\sim 1 \times 10^{13}$ photons/cm^2 pulse. (d) Temporal decay kinetics after excitation at the CT state (575 nm) of the XB and CT complex bleach of $(pyrene\text{-}C_4{:}TCNQ)_2PbI_4$ and the CT complex bleach of the organic (pyrene-C_4:TCNQ) CT complex.

investigated the changes in excited-state absorption by femtosecond transient absorption (fs-TA) measurements.[27]

To confirm formation of positive charges in the inorganic octahedral layers and the possible formation of TCNQ anions due to the electron localization in these molecules, we have performed fs-TA measurements to study the changes in absorption due to photoexcitation with a fast time resolution (~180 fs). These measurements were performed at various excitation wavelengths that correspond to the excitonic peak (~490 and 520 nm) and charge-transfer state (~575 nm) of $(pyrene\text{-}C_4{:}TCNQ)_2PbI_4$. The absorbed photon intensities were $\sim 1.3 \times 10^{13}$, $\sim 8.0 \times 10^{12}$, and $\sim 1.7 \times 10^{13}$ photons/cm^2 pulse, respectively. The transient changes in the optical absorption spectrum due to photoexcitation were detected using short broadband pulses obtained from continuum generation in a thick sapphire crystal (490−800 nm). As these measurements were performed in thin films, the TA absorption signals were corrected for changes in the reflection of the samples.

The TA spectra of $(pyrene\text{-}C_4)_2PbI_4$ photoexcited at 490 nm and $(pyrene\text{-}C_4{:}TCNQ)_2PbI_4$ photoexcited at 520 nm are shown in Figure 3a (full TA spectra in Figure S5). Both compounds exhibit the typical features observed for nonfunctional 2D perovskites as described in the literature: a bleach of the exciton band (XB) at ~495 nm for $(pyrene\text{-}C_4)_2PbI_4$ and ~530 nm for $(pyrene\text{-}C_4{:}TCNQ)_2PbI_4$, corresponding to band-edge filling by photogenerated excitons.[31] An additional photoinduced absorption (PA) is observed around the main XB feature, which has been attributed to band gap renormalization (BGR) due to exciton−exciton interactions.[31] Interestingly, the TA spectrum of $(pyrene\text{-}C_4{:}TCNQ)_2PbI_4$ exhibits an additional bleach between 550 and 750 nm (shown in the inset of Figure 3a). This bleach peaks at ~575 and ~650 nm and is in agreement with the ground-state absorption spectrum of this material shown in Figure 1b. As discussed above, these features correspond to the absorption of the (pyrene-C_4:TCNQ) CT complex. This clearly indicates that photoexcitation of the inorganic layers in the materials also leads to a bleach signal due the organic part, resulting from either direct excitation of the organic CT complex, charge transfer, or energy transfer.

To distinguish between charge and energy transfer, we have also performed fs-TA experiments by photoexciting the materials at 575 nm, where the absorption of the (pyrene-C_4:TCNQ) CT complex is centered. In Figure 3b, the TA spectra of $(pyrene\text{-}C_4{:}TCNQ)_2PbI_4$ upon photoexcitation at 520 and 575 nm and for the (pyrene-C_4:TCNQ) CT complex upon photoexcitation at 575 nm are shown. Full TA spectra are shown in Figure S6. Figure 3b shows that for both excitation wavelengths the TA spectrum of the (pyrene-C_4:TCNQ) CT complex closely matches with the ground-state absorption spectrum for this material shown in Figure 1b. The TA spectra for $(pyrene\text{-}C_4{:}TCNQ)_2PbI_4$ also show the bleach between 550 and 750 nm, both for excitation at 520 and 575

https://dx.doi.org/10.1021/acs.jpclett.9b03746
J. Phys. Chem. Lett. 2020, 11, 824−830

nm, even though the relative intensities of the different peaks differ slightly from the shape observed for (pyrene-C_4:TCNQ). This difference may arise from structural reorganization of the (pyrene-C_4:TCNQ) complexes between the inorganic octahedra.[29] Nevertheless, it is clear that a bleach feature is observed between 550 and 750 nm in Figure 3 for both excitation wavelengths, which is related to the high-energy charge-transfer bands of the (pyrene-C_4:TCNQ) CT complex.[27] Notably, in Figure 3b, it is also seen that when (pyrene-C_4:TCNQ)$_2$$PbI_4$ is excited at 575 nm (CT states from the complex) there is a fast-appearing feature in the TA spectrum that corresponds with the features seen for the exciton in the inorganic layers, centered at ∼530 nm. This clearly indicates that the initially created excited state does not remain localized on the organic CT complex. Because excited-state energy transfer is energetically not possible, the likely explanation is that hole transfer to the inorganic PbI_4 framework occurs, while the electron stays localized on TCNQ. It should be noted that the formation of the separated charges is induced by a built-in energy gradient between the inorganic layer and the CT complex state and not by decreasing the intrinsic exciton binding energy.[8,9] About this built-in energy gradient, we can directly conclude that the LUMO of TCNQ is inside the CB−VB gap of the inorganic layer, while the HOMO of the pyrene is below the CB band edge. However, consistent with the photoconductivity TRMC measurements, the magnitude of this feature is 1−2 orders of magnitude lower than when the main XB is directly excited. This supports the conclusion that this charge-transfer process is rather inefficient compared to the direct generation of excitons in the inorganic layer.

To gain insight into the populations of the different species as a function of time, the kinetics of the XB of (pyrene-C_4)$_2$$PbI_4$ upon photoexcitation at 490 nm and (pyrene-C_4:TCNQ)$_2$$PbI_4$ upon photoexcitation at both 520 and 575 nm are shown in Figure 3c. The decay observed for (pyrene-C_4)$_2$$PbI_4$ corresponds to the intrinsic decay of excitons localized in the inorganic octahedral layer. In (pyrene-C_4:TCNQ)$_2$$PbI_4$, the initial decay of the XB feature upon photoexcitation at 520 nm is considerably faster than in (pyrene-C_4)$_2$$PbI_4$. This may be related to the overlap with the decay of the excited states in the (pyrene-C_4:TCNQ) CT complex that also absorbs at 520 nm (decay time of ∼290 ps) or due to fast electron recombination as holes are injected from the organic CT complex into the inorganic layer.[27] The kinetics of the XB of (pyrene-C_4:TCNQ)$_2$$PbI_4$ excited at the CT state (575 nm) exhibit a similarly fast initial decay followed by a much longer component [>2.7 ns (Figure S7)]. The latter is attributed to the presence of long-lived charge-separated pairs, with an electron on TCNQ and a mobile hole in the inorganic layers giving rise to the long-lived photoconductivity signal in the microwave conductivity measurements. To confirm this, the temporal decay kinetics at the XB and CT complex bleach for (pyrene-C_4:TCNQ)$_2$$PbI_4$ and the (pyrene-C_4:TCNQ) CT complex are shown after excitation at the CT state (575 nm) (Figure 3d). In Figure 3d, the charge transfer from the CT complex is clearly observed in the kinetics. The XB and CT bleach in (pyrene-C_4:TCNQ)$_2$$PbI_4$ grow instantaneously but decay with a slower rate (lifetime of >1 ns) clearly exceeding the typical excited-state lifetimes of the organic CT complex (290 ps).[27] This is a direct consequence of the presence of the inorganic perovskite structure and hole transfer from the CT complex to the perovskite layer. As the electron and hole are separated in space, this state is non-emissive (PLQY = 0) as it was seen in the photoluminescence experiments and no EL is expected. The long-lived charges generated by charge separation between the CT complex and the inorganic layers have lifetimes that go well beyond the maximum delay time of the fs-TA experiment. As shown above in the TRMC experiments, these charges give rise to a very long-lived conductivity signal. It should be noted that a direct comparison of the time scales in the TA and TRMC experiments is not possible due to the very different time resolution and sensitivity of the two experiments.

In this work, we show, by a combination of microwave conductivity and transient absorption experiments, that introducing charge-transfer complexes between the inorganic layers of 2D perovskites leads to long-lived hole conduction in the inorganic octahedral layer after charge separation from the organic CT complex. While the yield of this charge-transfer process is relatively low and the transport of electrons is limited/trapped, this work reveals that charge separation can occur in solid-state 2D perovskites through the use of a functional organic layer. To improve the yield of the charge separation process and transport in the organic layer, a redesign of the organic molecules is necessary, for instance, decreasing the average distance between the organic chromophores and the inorganic layers and introducing organic moieties that form a continuous ordered pathway for charge transport, for example, introducing a (crystalline) n-type organic semiconductor such as perylene diimide molecules. Nevertheless, the results presented here show the high potential of including organic molecules with specific functionality in the 2D perovskites.

EXPERIMENTAL METHODS

Chemicals and Reagents. 7,7,8,8-Tetracyanoquinodimethane (TCNQ, >98.0%) was purchased from TCI. Potassium phthalimide salt (95%) was obtained from Fluorochem. Lead iodide (PbI_2, 99.999%) was obtained from Lumtec. 1-Pyrenebutyric acid (95%) was purchased from Combi-Blocks, Inc. Lithium aluminum hydride ($LiAlH_4$, 95%), carbon tetrabromide (CBr_4, 98%), potassium carbonate (K_2CO_3, ≥99%), magnesium sulfate ($MgSO_4$, 99%), ammonium chloride (NH_4Cl, ≥99%), triphenylphosphine (Ph_3P, 99%), pyrene (98%), hydrazine monohydrate (65%), potassium *tert*-butoxide (≥98%), and hydriodic acid (57 wt % aqueous solution) were purchased from Fisher Scientific. All chemicals were used without further purification. The dry dimethylformamide (DMF) that was used to make the precursor solutions and dry tetrahydrofuran (THF), which was used for the reactions, were obtained from our in-house solvent purification system (MBRAUN SPS-800). All other solvents were purchased from Fisher Scientific. The $PyrC_4NH_3I$ salt was synthesized as described in previous publications.[22,23]

Thin-Film Deposition.[22] Stoichiometric amounts of the respective precursors pyrene-C_n, TCNQ, and PbI_2 were dissolved in dry dimethylformamide (DMF) at 50−70 °C for 15 min while being constantly stirred. The resulting clear solutions were filtered through a syringe filter (0.45 mm pore size). Quartz substrates were cleaned through consecutive sonication steps in a series of solvents (detergent water, deionized water, acetone, and isopropanol) for 15 min each, followed by an ultraviolet−ozone treatment for 15 min. Films for optical measurements, TRMC, and XRD analysis were deposited on quartz substrates using spin coating in a glovebox with a nitrogen atmosphere (<0.1 ppm O_2, < 0.1 ppm H_2O) at

https://dx.doi.org/10.1021/acs.jpclett.9b03746
J. Phys. Chem. Lett. 2020, 11, 824−830

2000 rpm s^{-1} for 20 s. Subsequently, the films were post-annealed at temperatures between 110 and 150 °C. X-ray diffraction measurements were performed at room temperature in ambient atmosphere on a Bruker D8 Discover diffractometer with Cu Kα radiation.

Time-Resolved Microwave Photoconductivity (TRMC) Measurements. Samples for TRMC were placed in a sealed resonant cavity inside a helium-filled glovebox. Laser pulsed excitation (repetition rate of 10 Hz) at 335, 490, 525, 575, and 630 nm in a temperature range of 93−363 K. The photon intensities were varied over the range of 5×10^{13} to 3×10^{15} photons/cm^2 which correspond to concentrations of $\sim 6 \times 10^{17}$ and $\sim 2 \times 10^{19}$ cm^{-3}, respectively. The time resolution is limited by the width of the laser pulse (3.5 ns full width at half-maximum) and the response time of the system (18 ns).

Femtosecond Transient Absorption Spectroscopy. Pump−probe transient absorption measurements were performed using a tunable laser system comprising a Yb:KGW laser source (1028 nm) operating at 5 kHz (2.5 kHz repetition rate) with a pulse duration of 180 fs (PHAROS-SP-06-200, Light Conversion) and an optical parametric amplifier (ORPHEUS-PO15F5HNP1, light conversion). Probe light was generated by continuum generation, focusing a small fraction of the fundamental laser light in a thick sapphire crystal (~490−800 nm). The 2D data were acquired with a transient absorption spectrometer (HELIOS, Ultrafast Systems). The thin films were placed in an airtight sample holder loaded inside a helium-filled glovebox and excited at 490, 520, and 575 nm with pump fluences of $\sim 1.3 \times 10^{13}$, $\sim 8.0 \times 10^{12}$, and $\sim 1.7 \times 10^{13}$ photons/cm^2 pulse, respectively. The system is in quasi parallel pump−probe geometry with a 200 μm probe spot size. The measurements were performed in transmission and reflection and corrected with eq 1.

$$\Delta A = \log_{10}\left[10^{-\Delta A^*} + \frac{F_R}{1 - F_A}(10^{-\Delta R} - 10^{-\Delta A^*})\right] \quad (1)$$

where A is the absorbance, R the reflectance, T the transmission, and F_X the fractional X (X = A or R).

■ ASSOCIATED CONTENT

Supporting Information

The Supporting Information is available free of charge at https://pubs.acs.org/doi/10.1021/acs.jpclett.9b03746.

Additional XRD, TRMC, and TA experiments (PDF)

■ AUTHOR INFORMATION

Corresponding Author

Ferdinand C. Grozema − *Delft University of Technology, Delft, The Netherlands;* orcid.org/0000-0002-4375-799X; Email: F.C.Grozema@tudelft.nl

Other Authors

María C. Gélvez-Rueda − *Delft University of Technology, Delft, The Netherlands*

Wouter T. M. Van Gompel − *Hasselt University, Hasselt, Belgium;* orcid.org/0000-0002-8173-5206

Roald Herckens − *Hasselt University, Hasselt, Belgium*

Laurence Lutsen − *Associated Laboratory IMOMEC, Diepenbeek, Belgium*

Dirk Vanderzande − *Hasselt University, Hasselt, Belgium, and Associated Laboratory IMOMEC, Diepenbeek, Belgium;* orcid.org/0000-0002-9110-124X

Complete contact information is available at: https://pubs.acs.org/10.1021/acs.jpclett.9b03746

Notes

The authors declare no competing financial interest.

■ ACKNOWLEDGMENTS

The research leading to these results at the Delft University of Technology has received funding from European Research Council Horizon 2020 ERC Grant Agreement 648433. The FWO is acknowledged for the funding of the research. W.T.M.V.G. is an SB PhD fellow at FWO (1S17516N). R.H. is a special research fund (BOF) doctoral (PhD) student at UHasselt/IMO. The PVopMaat project funded by Interreg Vlaanderen-Nederland is acknowledged for funding. The synthesis of materials and films has been carried out in the context of the Solliance network (www.solliance.eu) and the EnergyVille consortium (http://www.energyville.be), of which Hasselt University is a member.

■ REFERENCES

(1) Straus, D. B.; Kagan, C. R. Electrons, Excitons, and Phonons in Two-Dimensional Hybrid Perovskites: Connecting Structural, Optical, and Electronic Properties. *J. Phys. Chem. Lett.* **2018**, *9* (6), 1434−1447.

(2) Mao, L.; Stoumpos, C. C.; Kanatzidis, M. G. Two-Dimensional Hybrid Halide Perovskites: Principles and Promises. *J. Am. Chem. Soc.* **2019**, *141* (3), 1171−1190.

(3) Ishihara, T. Optical Properties of PbI-Based Perovskite Structures. *J. Lumin.* **1994**, *60−61* (C), 269−274.

(4) Muljarov, E. A.; Tikhodeev, S. G.; Gippius, N. A.; Ishihara, T. Excitons in Self-Organized Semiconductor/Insulator Superlattices: PbI-Based Perovskite Compounds. *Phys. Rev. B: Condens. Matter Mater. Phys.* **1995**, *51* (20), 14370−14378.

(5) Mitzi, D. B.; Wang, S.; Feild, C. A.; Chess, C. A.; Guloy, A. M. Conducting Layered Organic-Inorganic Halides Containing -Oriented Perovskite Sheets. *Science* **1995**, *267* (5203), 1473−1476.

(6) Gélvez-Rueda, M. C.; Hutter, E. M.; Cao, D. H.; Renaud, N.; Stoumpos, C. C.; Hupp, J. T.; Savenije, T. J.; Kanatzidis, M. G.; Grozema, F. C. Interconversion between Free Charges and Bound Excitons in 2D Hybrid Lead Halide Perovskites. *J. Phys. Chem. C* **2017**, *121* (47), 26566−26574.

(7) Blancon, J. C.; Stier, A. V.; Tsai, H.; Nie, W.; Stoumpos, C. C.; Traoré, B.; Pedesseau, L.; Kepenekian, M.; Katsutani, F.; Noe, G. T.; et al. Scaling Law for Excitons in 2D Perovskite Quantum Wells. *Nat. Commun.* **2018**, *9* (1), 1−10.

(8) Cheng, B.; Li, T.-Y.; Maity, P.; Wei, P.-C.; Nordlund, D.; Ho, K.-T.; Lien, D.-H.; Lin, C.-H.; Liang, R.-Z.; Miao, X.; et al. Extremely Reduced Dielectric Confinement in Two-Dimensional Hybrid Perovskites with Large Polar Organics. *Commun. Phys.* **2018**, *1* (1), 80.

(9) Febriansyah, B.; Koh, T. M.; Lekina, Y.; Jamaludin, N. F.; Bruno, A.; Ganguly, R.; Shen, Z. X.; Mhaisalkar, S. G.; England, J. Improved Photovoltaic Efficiency and Amplified Photocurrent Generation in Mesoporous n = 1 Two-Dimensional Lead−Iodide Perovskite Solar Cells. *Chem. Mater.* **2019**, *31* (3), 890−898.

(10) Maheshwari, S.; Savenije, T. J.; Renaud, N.; Grozema, F. C. Computational Design of Two-Dimensional Perovskites with Functional Organic Cations. *J. Phys. Chem. C* **2018**, *122* (30), 17118−17122.

(11) Passarelli, J. V.; Fairfield, D. J.; Sather, N. A.; Hendricks, M. P.; Sai, H.; Stern, C. L.; Stupp, S. I. Enhanced Out-of-Plane Conductivity and Photovoltaic Performance in n = 1 Layered Perovskites through

Organic Cation Design. *J. Am. Chem. Soc.* **2018**, *140* (23), 7313−7323.
(12) Mitzi, D. B.; Chondroudis, K.; Kagan, C. R. Design, Structure, and Optical Properties of Organic-Inorganic Perovskites Containing an Oligothiophene Chromophore. *Inorg. Chem.* **1999**, *38* (26), 6246−6256.
(13) Dunlap-Shohl, W. A.; Barraza, E. T.; Barrette, A.; Dovletgeldi, S.; Findik, G.; Dirkes, D. J.; Liu, C.; Jana, M. K.; Blum, V.; You, W. Materials Horizons Tunable Internal Quantum Well Alignment in Rationally Designed Oligomer-Based Perovskite Matrix-Assisted Pulsed Laser Evaporation †. *Mater. Horiz.* **2019**, *6*, 1707−1716.
(14) Evans, H. A.; Labram, J. G.; Smock, S. R.; Wu, G.; Chabinyc, M. L.; Seshadri, R.; Wudl, F. Mono- and Mixed-Valence Tetrathiafulvalene Semiconductors (TTF)BiI4 and (TTF)4BiI6 with 1D and 0D Bismuth-Iodide Networks. *Inorg. Chem.* **2017**, *56* (1), 395−401.
(15) Evans, H. A.; Lehner, A. J.; Labram, J. G.; Fabini, D. H.; Barreda, O.; Smock, S. R.; Wu, G.; Chabinyc, M. L.; Seshadri, R.; Wudl, F. (TTF)Pb 2 I 5: A Radical Cation-Stabilized Hybrid Lead Iodide with Synergistic Optoelectronic Signatures. *Chem. Mater.* **2016**, *28* (11), 3607−3611.
(16) Mitzi, D. B.; Medeiros, D. R.; Malenfant, P. R. L. Intercalated Organic-Inorganic Perovskites Stabilized by Fluoroaryl-Aryl Interactions. *Inorg. Chem.* **2002**, *41* (8), 2134−2145.
(17) Mitzi, D. B. Templating and Structural Engineering in Organic−Inorganic Perovskites. *J. Chem. Soc. Dalt. Trans.* **2001**, No. 1, 1−12.
(18) Mitzi, D. B.; Medeiros, D. R.; Malenfant, P. R. L. Intercalated Organic-Inorganic Perovskites Stabilized by Fluoroaryl-Aryl Interactions. *Inorg. Chem.* **2002**, *41* (8), 2134−2145.
(19) Liu, C.; Huhn, W.; Du, K.-Z.; Vazquez-Mayagoitia, A.; Dirkes, D.; You, W.; Kanai, Y.; Mitzi, D. B.; Blum, V. Tunable Semiconductors: Control over Carrier States and Excitations in Layered Hybrid Organic-Inorganic Perovskites. *Phys. Rev. Lett.* **2018**, *121*, 146401.
(20) Hu, H.; Meier, F.; Zhao, D.; Abe, Y.; Gao, Y.; Chen, B.; Salim, T.; Chia, E. E. M.; Qiao, X.; Deibel, C.; Lam, Y. M. Efficient Room-Temperature Phosphorescence from Organic−Inorganic Hybrid Perovskites by Molecular Engineering. *Adv. Mater.* **2018**, *30* (36), 1707621.
(21) Hu, H.; Zhao, D.; Gao, Y.; Qiao, X.; Salim, T.; Chen, B.; Chia, E. E. M.; Grimsdale, A. C.; Lam, Y. M. Harvesting Triplet Excitons in Lead-Halide Perovskites for Roomerature Phosphorescence. *Chem. Mater.* **2019**, *31* (7), 2597−2602.
(22) Van Gompel, W. T. M.; Herckens, R.; Van Hecke, K.; Ruttens, B.; D'Haen, J.; Lutsen, L.; Vanderzande, D. Towards 2D Layered Hybrid Perovskites with Enhanced Functionality: Introducing Charge-Transfer Complexes via Self-Assembly. *Chem. Commun.* **2019**, *55* (17), 2481−2484.
(23) Van Gompel, W. T. M.; Herckens, R.; Van Hecke, K.; Ruttens, B.; D'Haen, J.; Lutsen, L.; Vanderzande, D. Low-Dimensional Hybrid Perovskites Containing an Organic Cation with an Extended Conjugated System: Tuning the Excitonic Absorption Features. *ChemNanoMat* **2019**, *5* (3), 323−327.
(24) Cao, D. H.; Stoumpos, C. C.; Farha, O. K.; Hupp, J. T.; Kanatzidis, M. G. 2D Homologous Perovskites as Light-Absorbing Materials for Solar Cell Applications. *J. Am. Chem. Soc.* **2015**, *137* (24), 7843−7850.
(25) Mao, L.; Tsai, H.; Nie, W.; Ma, L.; Im, J.; Stoumpos, C. C.; Malliakas, C. D.; Hao, F.; Wasielewski, M. R.; Mohite, A. D.; et al. Role of Organic Counterion in Lead- and Tin-Based Two-Dimensional Semiconducting Iodide Perovskites and Application in Planar Solar Cells. *Chem. Mater.* **2016**, *28* (21), 7781−7792.
(26) Stoumpos, C. C.; Cao, D. H.; Clark, D. J.; Young, J.; Rondinelli, J. M.; Jang, J. I.; Hupp, J. T.; Kanatzidis, M. G. Ruddlesden-Popper Hybrid Lead Iodide Perovskite 2D Homologous Semiconductors. *Chem. Mater.* **2016**, *28* (8), 2852−2867.
(27) Dillon, R. J.; Bardeen, C. J. Time-Resolved Studies of Charge Recombination in the Pyrene/TCNQ Charge-Transfer Crystal: Evidence for Tunneling. *J. Phys. Chem. A* **2012**, *116* (21), 5145−5150.
(28) Herckens, R.; Van Gompel, W. T. M.; Song, W.; Gélvez-Rueda, M. C.; Maufort, A.; Ruttens, B.; D'Haen, J.; Grozema, F. C.; Aernouts, T.; Lutsen, L.; et al. Multi-Layered Hybrid Perovskites Templated with Carbazole Derivatives: Optical Properties, Enhanced Moisture Stability and Solar Cell Characteristics. *J. Mater. Chem. A* **2018**, *6* (45), 22899−22908.
(29) Marchal, N.; Van Gompel, W.; Gélvez-Rueda, M. C.; Vandewal, K.; Van Hecke, K.; Boyen, H.-G.; Conings, B.; Herckens, R.; Maheshwari, S.; Lutsen, L.; et al. Lead-Halide Perovskites Meet Donor−Acceptor Charge-Transfer Complexes. *Chem. Mater.* **2019**, *31* (17), 6880−6888.
(30) Savenije, T. J.; Ferguson, A. J.; Kopidakis, N.; Rumbles, G. Revealing the Dynamics of Charge Carriers in Polymer:Fullerene Blends Using Photoinduced Time-Resolved Microwave Conductivity. *J. Phys. Chem. C* **2013**, *117* (46), 24085−24103.
(31) Li, Q.; Lian, T. Ultrafast Charge Separation in Two-Dimensional CsPbBr 3 Perovskite Nanoplatelets. *J. Phys. Chem. Lett.* **2019**, *10* (3), 566−573.

https://dx.doi.org/10.1021/acs.jpclett.9b03746
J. Phys. Chem. Lett. 2020, 11, 824−830